Dietary restriction of individual amino acids stimulates unique molecular responses in mouse liver

Spencer A. Haws[1,2], Yang Liu[3,4], Cara L. Green[3,4], Reji Babygirija[3,4,5], Eric A. Armstrong[1,2], Anusha T. Mehendale[1,2], Dudley W. Lamming[3,4,5,6*], and John M. Denu[1,2*].

[1]Wisconsin Institute for Discovery, University of Wisconsin-Madison, Madison, WI 53715, USA.
[2]Department of Biomolecular Chemistry, University of Wisconsin-Madison, Madison, WI 53706, USA.
[3]Department of Medicine, University of Wisconsin-Madison, Madison, WI 53705, USA.
[4]William S. Middleton Memorial Veterans Hospital, Madison, WI 53705, USA.
[5]Graduate Program in Cellular and Molecular Biology, University of Wisconsin-Madison, Madison, WI 53706, USA
[6]University of Wisconsin Carbone Comprehensive Cancer Center, University of Wisconsin, Madison, WI 53705, USA.

[*]**Correspondence**
Dudley W. Lamming, PhD
Associate Professor of Medicine
University of Wisconsin-Madison
1685 Highland Ave
MFCB Rm 4147
Madison, WI 53705, USA
dlamming@medicine.wisc.edu
Tel: 608-262-7341

John M. Denu, PhD
Professor of Biomolecular Chemistry
john.denu@wisc.edu

Abstract

Dietary protein and essential amino acid (EAA) restriction promotes favorable metabolic reprogramming, ultimately resulting in improvements to both health and lifespan. However, as individual EAAs have distinct catabolites and engage diverse downstream signaling pathways, it remains unclear to what extent shared or AA-specific molecular mechanisms promote diet-associated phenotypes. Here, we investigated the physiological and molecular effects of restricting either dietary methionine, leucine, or isoleucine (Met-R, Leu-R, and Ile-R) for 3 weeks in C57BL/6J male mice. While all 3 AA-depleted diets promoted fat and lean mass loss and slightly improved glucose tolerance, the molecular responses were more diverse; while hepatic metabolites altered by Met-R and Leu-R were highly similar, Ile-R led to dramatic changes in metabolites, including a 3-fold reduction in the oncometabolite 2-hydroxyglutarate. Pathways regulated in an EAA-specific manner included glycolysis, the pentose phosphate pathway (PPP), nucleotide metabolism, the TCA cycle and amino acid metabolism. Transcriptiome analysis and global profiling of histone post-translational modifications (PTMs) revealed different patterns of responses to each diet, although Met-R and Leu-R again shared similar transcriptional responses. While the pattern of global histone PTMs were largely unique for each dietary intervention, Met-R and Ile-R had similar changes in histone-3 methylation/acetylation PTMs at lysine-9. Few similarities were observed between the physiological or molecular responses to EAA restriction and treatment with rapamycin, an inhibitor of the mTORC1 AA-responsive protein kinase, indicating the response to EAA restriction may be largely independent of mTORC1. Together, these results demonstrate that dietary restriction of individual EAAs has unique, EAA-specific effects on the hepatic metabolome, epigenome, and transcriptome, and suggests that the specific EAAs present in dietary protein may play a key role at regulating health at the molecular level.

Keywords: methionine, leucine, isoleucine, epigenetic, post-translational modification, protein restriction

Introduction

Dietary protein is a key regulator of metabolism, health, and even longevity (Green et al., 2022). It has long been suspected that the health benefits of a low protein diet arise not simply due to the consumption of reduced protein, but due to decreased levels of specific amino acids. For many years, attention has focused on the potential role of dietary methionine in regulating metabolism and health. Plant-based protein may have reduced levels of methionine compared to animal proteins, and vegans have lower than normal plasma levels of methionine; thus, many have attributed the health benefits of a vegan diet to decreased consumption of methionine (MacArthur et al., 2021; McCarty et al., 2009; Schmidt et al., 2016). The potential metabolic benefits of reduced methionine intake are readily observed in rodents, where restriction of methionine extends lifespan, promotes leanness and insulin sensitivity, and promotes the rapid loss of adipose tissue and improved glycemic control in diet-induced obese mice (Miller et al., 2005; Orentreich et al., 1993; Sun et al., 2009; Wanders et al., 2017; Yu et al., 2018).

However, methionine is only one of the twenty common amino acids, and there is a growing awareness that other dietary essential amino acids have critical roles in regulating metabolism. The most well-known of these are the branched-chain amino acids (BCAAs; leucine, isoleucine, and valine), which are elevated in individuals with diabetes, are associated with insulin resistance in humans and rodents, and which promote insulin resistance in rats when supplemented in the diet (Newgard et al., 2009). Conversely, dietary restriction of the BCAAs promotes glucose tolerance, insulin sensitivity, and reduces adiposity in mice and rats (Cummings et al., 2018; Fontana et al., 2016; White et al., 2016). BCAA intake also regulates the lifespan of mice, with BCAA restriction extending the lifespan of mice and promoting lifelong leanness, and BCAA supplementation shortening lifespan and promoting obesity (Richardson et al., 2021; Solon-Biet et al., 2019).

Metabolism and the epigenome are connected by central metabolites that, in addition to their direct metabolic roles, act as co-substrates for chromatin-modifying enzymes (Fan et al., 2015; Li et al., 2018). Methionine is absolutely essential for the production of S-adenosylmethionine (SAM), which acts as a methyl donor for methyltransferases, and reduced SAM availability is associated with site-specific decreases in histone methylation (Haws et al., 2020).

Similarly, the BCAAs are catabolized either to acetyl-CoA (leucine), propionyl-CoA (valine), or both (isoleucine), and while having many other biological roles these BCAA-derived catabolites can be used for posttranslational modification of histones. Acetyl-CoA is required for histone acetylation, and acetyl-CoA derived from leucine can be utilized by the p300 histone acetyltransferase to acetylate multiple substrates (Son et al., 2019; Vermeulen et al., 2010); it was recently shown that isoleucine-derived propionyl-CoA is required for propionylation of cardiac H3K23 (Yang et al., 2023). The effects of leucine and isoleucine are particularly interesting as recent work has shown that restriction of leucine and isoleucine have dramatically different effects on the metabolic health of mice, with restriction of isoleucine being necessary and sufficient for the metabolic benefits of protein restriction including reduced adipose tissue, increased energy expenditure, and improved

glycemic control, while reducing leucine did not (Yu et al., 2021). Further, dietary levels of isoleucine, but not leucine, are associated with body mass index in humans (Yu et al., 2021).

It is thus clear that adaptive mechanisms exist that allow animals to actively respond not just to times of famine, but to decreased availability of specific essential amino acids. These may occur over different time periods, including meal to meal variation or simply during the day in response to feeding and circadian rhythm. Some of these mechanisms could involve the mechanistic Target of Rapamycin Complex 1 (mTORC1), an evolutionarily conserved sensor of amino acids that promotes growth and anabolic metabolism when amino acids are sufficient (Simcox and Lamming, 2022). We recently showed that restriction of dietary methionine could rapidly deplete methyl-metabolites, leading to a robust, conserved chromatin response characterized by broad decreases in di- and tri-methyl histone methylation as well as new monomethylation at specific sites (Haws et al., 2020). Many questions remain, including how the response to methionine depletion, which uniquely directly lowers SAM levels, compares to the effect of depleting other essential amino acids on the metabolome and epigenome.

Here, we investigate the metabolic effects of restricting methionine, leucine, and isoleucine on the physiology and the liver metabolome, epigenome, and transcriptome of C57BL/6J male mice. We further examined the potential role of mTORC1 in these responses by treating mice with rapamycin, an inhibitor of mTORC1. We find that restriction of each essential amino acid induces a pattern of unique effects, with isoleucine restriction consistently inducing the strongest and most distinct effects on the metabolome, epigenome and transcriptome. Surprisingly, despite restriction of methionine and leucine resulting in very distinct unique catabolites (SAM and acetyl-CoA, respectively), methionine restricted and leucine restricted animals showed the strongest similarity in their metabolomic and transcriptomic effects, suggesting that both strongly engage a shared pathway sensing deficiency of essential amino acids. However, among global PTMs changes on histones, methionine and isoleucine restriction yielded very similar methylation/acetylation trends on several sites on histone H3, suggesting a common set of chromatin modifying enzymes might regulate these distinct transcriptional responses. Finally, these response pathways may be independent of mTORC1, as the impact of rapamycin on the metabolome, epigenome, and transcriptome do not mimic the effect of restricting other essential amino acids. In conclusion, our results demonstrate that dietary restriction of each essential amino acid has unique, amino acid specific impacts on physiology and the liver metabolome, epigenome, and transcriptome, and suggest that the specific amino acid profile of dietary protein plays a key role at regulating not only health, but molecular processes.

Results

Essential amino acid restrictions elicit systemic physiologic responses unique from rapamycin treatment

To investigate how complete dietary restriction of essential amino acids subsequently impacts different physiologic measurements, we placed C57BL/6J 14-week-old male mice on one of four AA-defined diets for 3 weeks (**Fig. 1A**). Briefly, we utilized a widely utilized commercially available AA-defined Control diet in which 15.6% of calories are derived from AAs. We also utilized diets in which either methionine (Met-R), leucine (Leu-R), or isoleucine (Ile-R) were depleted. All of the diets are isocaloric, with identical levels of fat and carbohydrate; in each restricted diet, non-EAAs were increased to keep the calories derived from AAs constant. The full diet formulation for all diets are provided in **Table S1**. In parallel, a subset of Control-fed mice were also treated daily with rapamycin (**Fig. 1A**), an inhibitor of the mTORC1 (mechanistic Target Of Rapamycin Complex 1) protein kinase which acts as a key sensor of AAs. This was to enable us to see if mTORC1 inhibition would mimic the effects of EAA restriction; if so, this would implicate AA sensing by mTORC1 as a mediator of the physiological and molecular effects of EAA restriction.

We found that restriction of EAAs, but not rapamycin treatment, led to a steady decrease in total body weight over the course of the study (**Fig. 1B**). Met-R and Leu-R mice exhibited a similar pattern of lost body weight, weighing 7.5 g and 9.0 g less, respectively, than Control-fed mice following 3 weeks of EAA restriction. Notably, Ile-R mice lost significantly more body weight than both Met-R and Leu-R mice, weighing on average 12.25 g less than controls at the study's conclusion. The observed changes in body weight were largely independent of altered food intake patterns (**Fig. 1C**). Together, these data suggest 3 weeks of individual EAA restriction is sufficient to induce whole body weight loss, likely via increased energy expenditure as has been previously reported in similar systems[refs].

With changes in body weight largely driven by alterations to lean and fat mass stores, we performed whole body MRI analysis of each mouse at weeks 0 and 3 to identify any possible associated changes in body composition. This analysis revealed that only control mice retained lean mass over the course of our study. Rapamycin-treated mice displayed a minimal yet significant loss in lean mass while EAA restricted mice experienced an even greater lean mass loss (**Fig. 1D**). In addition to lean mass, EAA restriction also induced significant losses in fat mass. Met-R mice lost an average fat mass of 0.84 g per mouse with dietary restriction of either BCAA (i.e., Leu or Ile) having significantly greater effects (**Fig. 1E**). Specifically, Leu-R mice lost 1.5 g of fat per mouse while there was a near total loss in detectable fat mass for Ile-R mice. This loss in fat mass for Leu-R and Ile-R mice was greater in magnitude than the observed losses in lean mass, resulting in an altered body composition consisting of increased lean mass and decreased fat mass percentages (**Figs. 1F-G**). The relative percentages of lean and fat mass were unchanged in Met-R mice, while control and rapamycin treated mice exhibited increased fat mass which is consistent with normal age-associated changes in body composition. Therefore, these data show dietary restriction of individual BCAAs has a greater impact on body composition than Met-R, likely via mTOR-independent mechanisms.

In addition to altered body composition, dietary EAA restriction has also been associated with improved glucose tolerance. Although 3 weeks of complete dietary Met-R was unable to significantly improve glucose tolerance relative to controls, Leu-R and Ile-R mice exhibited improved glucose clearance under glucose tolerance test (GTT) conditions (**Figs. 1H-I**). These effects of EAA restriction were counter to those observed in rapamycin treated mice which displayed reduced glucose tolerance as has been previously observed[refs]. Together, these data show 3 weeks of individual EAA dietary restriction is sufficient to induce whole-organism physiologic changes, with each EAA restriction eliciting distinct phenotypes which cannot be replicated by rapamycin treatment alone.

Central metabolites and auxiliary cofactors are differentially regulated in response to individual dietary EAA restriction or rapamycin treatment

While dietary restriction of individual EAAs was able to elicit distinct physiologic phenotypes, we sought to determine whether such distinctions could be observed at the level of cellular metabolism. To do so, we performed a targeted liquid chromatography mass spectrometry (LC-MS) metabolomics analysis of liver tissue harvested at the study's conclusion. Hierarchical clustering of treatment groups based on the altered relative abundance of over 100 quantifiable metabolites revealed changes induced by dietary EAA restriction that were again more similar to one another than those stimulated by rapamycin (**Figs. 2A-B**). However, unlike the grouping patterns observed in our physiologic measurements, Leu-R mice exhibited a metabolic profile which more closely mimicked Met-R than Ile-R mice. This result was largely unexpected as methionine, a non-BCAA, possesses drastically different metabolic roles than either leucine or isoleucine. Therefore, these data suggest dietary methionine and leucine availability may act on shared amino acid sensing pathways in mouse liver while isoleucine signaling occurs through unique mechanisms.

To assess how dietary restriction of EAAs or rapamycin treatment altered cellular liver metabolism at a greater resolution, we assessed the relative changes of key metabolites in the larger context of their associated metabolic networks (**Figs. 2C-F**). With rapamycin, the most dramatic alteration occurred in the pentose phosphate pathway (PPP), where treated mice exhibited a large 4-fold elevation in ribulose 5-phosphate (R5P) (**Fig. 2C**) and corresponding 3-fold decrease of ribose 5-phosphate, indicating decreased metabolite flux through non-oxidative PPP metabolism. These metabolic changes are consistent with a recent report showing that mTORC1 positively controls the translation of ribose-5-phosphate isomerase A, the enzyme that interconverts ribulose 5-phosphate and ribose 5-phosphate (Buj et al., 2019). Opposingly, Ile-R mice possessed significantly lower R5P levels along with a greater availability of ribose 5-phosphate and downstream PPP metabolic products. Notably, Leu-R and Met-R mice exhibited this similar trend in PPP metabolite levels, suggesting increased PPP metabolism may be a shared response to dietary EAA restriction. Such shared patterns were less apparent when assessing glycolytic intermediates downstream of glucose 6-phosphate (G6P). A trending or significant increase in dihydroxyacetone phosphate (DHAP) was observed in all treatment groups although only Ile-R mice displayed an increased abundance of the downstream metabolite phosphoenolpyruvate (PEP). Conversion of PEP to pyruvate appeared uniquely reduced in Met-R mice as pyruvate, lactate, and acetyl-CoA

levels were significantly lower than controls. Although only Met-R mice showed decreased liver pyruvate levels, all treatments besides Ile-R stimulated a decrease in acetyl-CoA levels relative to controls (**Fig. 2D**). Similar trends were observed for propionyl- and butyryl-CoA, highlighting a general decrease in liver short chain acyl-CoA levels with rapamycin, Met-R, and Leu-R mice. However, decreased acetyl-CoA availability did not impact the initial entry of carbons into the TCA cycle as nearly all conditions displayed increased liver citrate levels. Only Met-R citrate levels were not significantly greater than controls, although a trending increase was observed. Curiously, elevated citrate levels did not correspond with a greater abundance of immediate downstream TCA cycle intermediates. All conditions exhibited similar or decreased abundance of cis-aconitate, alpha-ketoglutarate (alpha-KG), and/or succinate relative to controls. 2-hydroxyglutarate (2-HG), a metabolite with structural similarities to alpha-KG, was also significantly decreased in Ile-R mice. This apparent downregulation of TCA cycle metabolism was relieved in all conditions as fumarate and malate were significantly elevated in Met-R, Leu-R, and Ile-R mice with rapamycin treated mice exhibiting similar levels relative to controls. The increase in malate/fumarate may be driven by amino acid anaplerosis as increases in tyrosine and phenylalanine abundance mirrored those of malate and fumarate across all conditions. In addition to malate and fumarate, numerous other amino acids were generally elevated in response to any dietary EAA restriction, but not rapamycin treatment (**Figs. 2A and 2D**). In fact, the EAA designated for dietary restriction uniformly presented with elevated liver availability. As we have previously observed 5 weeks of Met-R is sufficient to lower liver methionine availability by greater than 50% (Haws et al., 2020), this result suggests metabolome responses to 3 weeks of dietary EAA restriction are likely to be driven by adaptive mechanisms meant to compensate for decreased dietary intake. Together, these data show glycolysis, PPP, and amino acid metabolism are susceptible to EAA- or rapamycin-specific regulation while TCA Cycle metabolism appears similarly affected across conditions.

In addition to central metabolites, several auxiliary metabolites that function as critical cofactors also showed differential regulation in response to dietary EAA restrictions or rapamycin treatment. For example, Ile-R led to the accumulation of high energy state adenosine and guanosine nucleotides (i.e, ATP and GDP) which showed a trending or significant decrease across the other treatment groups (**Fig. 2E**). Uridine, cytidine, and inosine nucleotides were also elevated in Ile-R mice with no clear pattern observed in response to other dietary EAA restrictions or rapamycin treatment. Interestingly, the redox metabolites NAD^+/NADH and $NADP^+$/NADPH were significantly reduced across all conditions, suggestive of an overall decrease in NAD^+ synthesis or increase in NAD catabolism (**Fig. 2F**). Relative abundance of the redox metabolites glutathione (GSH) and glutathione disulfide (GSSG) where unchanged in rapamycin-treated or Ile-R mice, with a decreased ratio of GSH to GSSG observed in Met-R and Leu-R mice. Therefore, these data show dietary Ile-R has a unique impact on the relative levels of auxiliary metabolic cofactors with dietary Met-R and Leu-R stimulating shared responses unique from both Ile-R and rapamycin-treated mice. Collectively, these observations further highlight the condition-specific effects of dietary EAA restrictions or rapamycin treatment on liver metabolism.

Dietary EAA restrictions stimulate unique Histone PTM patterns across all conditions, independent of mTORC1 regulation

Fluctuations in metabolite availability can regulate cellular processes through numerous, diverse mechanisms. One such mechanism includes direct regulation of the epigenome, as the enzymes responsible for 'writing' and 'erasing' epigenetic post-translational modifications (PTMs) rely on metabolic cofactors to support their catalytic activity. Notably, all three EAAs investigated in this study have distinct connections to such cofactors. For example, methionine is the immediate precursor to S-adenosylmethionine (SAM), the universal methyl-donor which supports all chromatin methylation reactions. As BCAAs, neither leucine or isoleucine have any direct links to SAM metabolism but can be metabolized to acetyl-CoA or acetyl-CoA/propionyl-CoA, respectively. These short chain acyl-CoAs can then directly support chromatin acylation reactions. Therefore, it is plausible that unique regulation of epigenetic post-translational modifications may accompany the unique transcriptional states associated with each intervention. Moreover, one of the largest gene enrichment sets for Ile-R was gene histone/protein posttranslational modifications.

To determine whether the liver epigenome is uniquely sensitive to dietary EAA restrictions or rapamycin treatment, we performed LC-MS/MS histone proteomics analyses on liver tissue harvested at the study's completion. Hierarchical clustering based on the altered relative abundance of over 60 unique histone peptides containing residues directly linked with transcriptional regulation revealed distinct histone PTM profiles for all treatment groups (**Figs. 3A-B**). We have previously investigated the epigenetic responses to Met-R in detail, revealing adaptive chromatin mechanisms highlighted by preferential H3K9me1 maintenance in the presence of global decreases to higher-state histone methylations (Haws et al., 2020). This observation was replicated in the present study, further underscoring its high level of conservation (**Fig. 3C**). Unexpectedly, Ile-R also exhibited an identical trend in H3K9 methylation states. Ile-R mice were also similar to Met-R mice regarding H3 acylation levels, displaying increased acetylation on H3K9/K14 and increased propionylation on both H3K9/K14 and H3K18/K23 (**Figs. 3C**-D). Similar trends in H3 acylation states were also observed in Leu-R mice, though rapamycin treatment only stimulated a significant increase in H3K9/K14 propionylation. Interestingly, the general increase in H3 acylations for Met-R and Ile-R mice was not observed on H4 residues, where significant decreases in acetylation were observed (**Fig. 3F**). While Met-R mice displayed decreased liver acetyl-CoA levels, Ile-R acetyl-CoA levels were unchanged. These data either suggest independent mechanisms dictate H4ac profiles in response to dietary Met-R/Ile-R, or that H4 acetylation mechanisms are shared but function independent of whole-cell acetyl-CoA availability. In support of the latter, H4 acetylation levels in Leu-R and rapamycin treated mice were robust despite decreased liver acetyl-CoA availability. Notably, unlike H4 acetylation levels, H4 short chain acylations were largely unchanged across conditions with only Ile-R mice exhibiting slight increases in butyrylated and crotonylated H4 residues (**Fig. 3G**). Together, these data demonstrate that dietary EAA restrictions or rapamycin have differential effects on the liver epigenome, providing a potential mechanism for EAA restriction-specific phenotypes.

Treatment-dependent alterations to liver transcriptional profiles mirror grouping patterns observed in metabolomics analyses with Ile-R stimulating the most significant response

Histone proteomics analyses following 3 weeks of dietary EAA restriction or rapamycin treatment demonstrated that liver epigenomes were fundamentally altered. Therefore, to identify how these alterations impacted the functional gene expression landscape of the liver, we performed bulk RNA-sequencing. Unexpectedly, principal component analysis (PCA) of log transformed gene counts per million (CPM) values revealed identical groupings to those observed in the metabolomics, but not histone PTMs (Figure 4A). As such, these data suggest a majority of the transcriptional adaptation to Met-R and Leu-R occurs through general amino acid sensing pathways with Ile-R again acting through unique mechanisms. In support of this observation, 45.6% (n = 4088) of all differentially expressed (DE) genes identified in Ile-R liver were uniquely altered under this condition alone (**Fig. 4B**). Only 11.7% (n=590) and 13.2% (n=494) of DE genes in Leu-R and Met-R mice, respectively, were unique to each given condition. In fact, a majority of Leu-R or Met-R DE genes were also differentially regulated by at least one other dietary EAA restriction (i.e., Leu-R = 83%, Met-R = 81.4%). Regarding rapamycin DE genes, 77.5% were also shared by at least one other EAA restricted condition. However, relative to the changes observed in other conditions, the absolute number of DE genes contributing to this pattern (n=478) was significantly lower. Therefore, these data suggest the transcriptional programs induced by dietary EAA restrictions likely occur largely independently of mTOR regulation.

In addition to identifying genes with unique or shared regulation across conditions, assessing the relative magnitude of DE gene profiles is also important for understanding the level of transcriptional adaptation that may have occurred. Volcano plots revealed a graded transcriptional response to dietary EAA restrictions or rapamycin treatment that again mirrored both physiologic and metabolomic results (**Figs. 4C-F**). Rapamycin treatment had a relatively minimal effect on gene expression profiles with the lowest log2 FC and -log10 adjusted p-values of any treatment group (**Fig. 4C**). Met-R and Leu-R livers exhibited an overall similar impact on gene expression profiles that were significantly greater than those from rapamycin treated mice although Leu-R samples did contain 35% more DE genes overall (**Figs. 4D-E**). Notably, Ile-R stimulated the greatest liver transcriptional response by far, both in terms of log2 FC and -log10 adjusted p-value magnitude as well as absolute DE gene number (**Figs. 4F**). Together, these data further highlight how dietary EAA restrictions stimulate unique transcriptional responses independent of mTOR regulation.

To continue assessing the unique transcriptional responses stimulated by each EAA restriction or rapamycin treatment in greater detail, DE genes previously determined to be specific to each given condition were used for Gene Ontology Biological Process (GO-BP) pre-ranked Gene Set Enrichment Analysis (GSEA) (**Figs. 4G-J, Table S2**). In line with the lower magnitude transcriptional response identified in rapamycin-treated mice, GSEA of rapamycin-specific DE genes produced very few significantly enriched gene sets (n=5). Significantly enriched gene sets that were identified all possessed negative normalized enrichment scores (NES) and primarily consisted of immunity related transcriptional programs (**Fig. 4G**). Although Met-R-specific DE genes were found to be enriched in a similar number of gene sets (n=6) as rapamycin treated mice, significantly enriched gene sets primarily possessed positive NES values and largely consisted of membrane organization/cell motility biological processes (**Fig. 4H**). Significantly enriched Leu-R gene sets (n=11)

predominantly held positive NES scores as well. Positive NES gene sets were overwhelmingly associated with diverse intracellular signal transduction pathways (**Fig. 4I**). Ile-R-specific DE genes were found to be significantly enriched in the greatest number of GO-BP gene sets (n=74) (**Fig. 4J**). Interestingly, multiple positive NES gene sets were associated with histone/protein posttranslational modifications, providing potential insights into mechanisms promoting a unique histone PTM profile in Ile-R mice. Negative NES gene sets were primarily associated with lipid metabolism and mitochondrial oxidative phosphorylation, suggestive of a compensatory mechanism aimed towards preserving liver lipid stores in the presence of a near complete loss in total fat mass. Therefore, these data reveal that of all dietary EAA restrictions tested, Ile-R stimulates the most unique transcriptional programs with the greatest magnitudes of change in mouse liver.

Discussion

In this study we set out to gain new insight into the molecular mechanisms by which dietary AA restrictions regulate metabolic physiology, using mice as a model and focusing on Ile, Leu and Met.

As predicted from prior work, Ile, Leu and Met restriction individually led to improved glucose tolerance and loss of fat and lean mass. Molecular assessment of each treatment led to surprising findings that highlighted both key differences and unique similarities. Isoleucine restriction yielded the most profound changes among the various groups, both in breadth and magnitude of changes. Increases in glycolytic and PPP intermediates was prominent, as was the increase in high-energy nucleotides. Together these observations suggest increased glucose flux through the PPP pathway, which could lead to greater glucose clearance. Although less dramatic, both Met-R and Leu-R tended to show similar increased PPP metabolites. It has been estimated that as much as ⅓ of incoming glucose can be consumed by the PPP (Hostetler and Landau 1967; Lee et al. 2019).

We were surprised to find that leucine and methionine restriction resulted in highly similar effects on metabolite levels and gene expression, suggesting that a common mechanism might be at play in sensing deficiency of these two EAAs. Although isoleucine restriction had quite distinct effects on gene expression compared with Leu-R and Met-R, trends in methylation/acylation on several histone H3 sites were shared between Ile-R and Met-R, suggesting that a common set of chromatin modifying enzymes might be engaged by restriction of methionine and isoleucine. It is important to note that the GO term “histone modification” was most highly enriched among the pathways unique to Ile-R, suggesting that regulation of histone modifying/PTM-associated genes could provide a newly adaptive epigenetic landscape that could persist after Ile repletion. Ongoing studies are targeting this question of persistence after restriction.

Ile-R led to a large 3-fold reduction in 2-HG (2-hydroxyglutarate) abundance while alpha-ketoglutarate was unchanged (**Fig. 2D**). Alpha-ketoglutarate serves as a co-substrate while 2-HG can directly inhibit the jumonji-containing domain histone demethylases, suggesting the possibility that the general histone hypomethylation phenotype observed with Ile-R results from higher rates of histone demethylation. The common features of H3K9 methylation changes under both Ile-R and Met-R are striking. We speculate that Ile-R and Met-R lead to reduced H3K9 methylation through two distinct pathways involving direct metabolic

control. With Met-R, lowered SAM levels reduce the capacity to maintain the higher methylation states, and with Ile-R, the significant reduction in 2HG allows the demethylases to operate at higher rates. We have mathematically modeled the relationship between H3K9 methyltransferases and demethylases under limiting MET/SAM and found this model to accurately depict the dynamics of H3K9 (de)methylation (Haws et al. 2023).

In recent published work, we investigated the epigenetic responses to Met-R in detail, revealing adaptive chromatin mechanisms highlighted by preferential H3K9me1 maintenance in the presence of global decreases to higher-state histone methylations (Haws et al., 2020). We proposed that active monomethylation at H3K9 provides an important place holder until SAM levels are restored and heterochromatin can be silenced through higher order methylation. Here, Ile-R exhibited an identical trend in H3K9 methylation states, and importantly Ile-R and Met-R treatments also yielded similar increased acetylation on H3K9/K14 and increased propionylation on both H3K9/K14 and H3K18/K23. Interestingly, the general increase in H3 acylations in Met-R and Ile-R mice was not observed on H4 residues, where instead significant decreases in acetylation were observed. While Met-R mice displayed decreased liver acetyl-CoA levels, Ile-R acetyl-CoA levels were unchanged. Collectively, there was no general trend in acetyl-CoA levels and the abundance of global histone acetylation, though some specific lysines exhibited a correlation. It is important to note that these measurements were made at 3 weeks restriction in a tissue that must adapt to whole body metabolic homeostasis. At this duration, the metabolome analysis indicated that the liver is not experiencing an EAA deficit, and accordingly, there is not a significant deficit in acetyl-CoA derived from dietary loss of Ile and Leu. All three EAA restrictions led to a general increase in free amino acids in the liver, even among the amino acids being restricted. These results, which are accompanied by a progressive decline in lean mass, are consistent with skeletal muscle loss (autophagy), freeing up EAAs for essential protein synthesis and other metabolic processes throughout the body. In the present three week study, steady-state liver methionine levels are not yet decreased in Met-R animals. In prior studies, we have shown that after 5 weeks of Met-R methionine levels drop 2-fold (Green et al., 2023; Yu et al., 2021). An important trend observed in the EAA restrictions is the liver's self preservation. This is most apparent in genes being downregulated. Genes involved in autophagy, electron transport chain (ETC), fatty acid (FA) catabolism, and BCAA catabolism are reduced by EAA restriction, consistent with the maintenance of liver function and sacrificing skeletal muscle and fat stores.

We also examined the effects of mTOR inhibition. Rapamycin treatment as a separate arm was included to assess whether the observed molecular phenotypes were consistent with involvement of the canonical mTOR nutrient-sensing pathway. Overall, our analysis of the metabolomic, epigenetic, and transcriptomic effects of rapamycin suggest that this treatment is distinct from the effects of EAA restriction, and imply that inhibition of the mTOR signaling pathway is playing a minor role in the response to EAA restriction. A potential limitation of this conclusion is that there are rapamycin-resistant functions of mTORC1 that could be engaged by EAA restriction (Thoreen et al., 2009), and additional work with genetically engineered mouse models of altered mTORC1 signaling will be needed to confirm that EAAs function through a mTORC1-independent pathway.

In conclusion, we have shown that dietary restriction of a single EAA, while having somewhat similar effects at the physiological level, have both diverse and overlapping molecular effects at the level of the

metabolome, epigenome, and transcriptome. Intriguingly we found strong similarities between the effects of Met-R and Leu-R on the metabolome and transcriptome, while restriction of Ile led to dramatic changes in both hepatic metabolites and gene expression. While the pattern of global histone PTMs were distinct to each dietary intervention, Met-R and Ile-R induced similar changes in histone-3 methylation/acetylation PTMs at lysine-9. While the data are consistent with EAA restriction inducing molecular effects independent of mTORC1, the exact molecular mechanisms that mediate these effects remain to be identified. Our results showing large changes in metabolism, gene expression and the epigenetic landscape demonstrate that single EAA restrictions have profound effects on hepatic function, and highlight both the similarities and differences among Met, Leu and Ile.

Methods

Animals and Diets

All procedures were performed in conformance with institutional guidelines and were approved by the Institutional Animal Care and Use Committee of the William S. Middleton Memorial Veterans Hospital (Madison, WI, USA). Male C57BL/6J (#000664) mice were obtained from The Jackson Laboratory. All mice were housed three per cage, maintained at a temperature of approximately 22°C, and health checks were completed on all mice daily. Studies were commenced when the mice were 14 weeks of age.

Mice were then randomized to receive the indicated diets from Inotiv either the Control (TD.01084), Met-R (TD.140119), Leu-R (TD.180789) or Ile-R (TD.190879) diets, or the Control diet plus rapamycin (delivered 4 mg/kg/day I.P. as described (Arriola Apelo et al., 2016)). Full diet descriptions are provided in Table S1. The randomization of mice was performed at the cage level to ensure that all groups had approximately the same initial starting weight and body composition. Mice were housed in a SPF mouse facility in static microisolator cages, except when temporarily housed in a Columbus Instruments Oxymax/CLAMS metabolic chamber system. Mice were housed under a 12:12 h light/dark cycle with free access to food and water, except where noted in the procedures below.

In vivo Procedures

Glucose tolerance tests were performed by fasting the mice overnight for 16 hours and then injecting glucose (1 g kg^{-1}) (Bellantuono et al., 2020; Yu et al., 2018). Glucose measurements were taken using a Bayer Contour blood glucose meter (Bayer, Leverkusen, Germany) and test strips. Mouse body composition was determined using an EchoMRI Body Composition Analyzer (EchoMRI, Houston, TX, USA). For assay of multiple metabolic parameters [O2, CO2, food consumption, respiratory exchange ratio (RER), energy expenditure] and activity tracking, mice were acclimated to housing in a Oxymax/CLAMS metabolic chamber system (Columbus Instruments) for ~24 h and data from a continuous 24 h period was then recorded and analyzed. Food consumption in home cages was measured by moving mice to clean cages, filling the hopper with a measured quantity of fresh diet in the morning and measuring the remainder in the morning 3 days later. The amount was adjusted for the number of mice per cage, the number of days that passed and the relative weights of the mice (i.e., heavier mice were credited with a larger relative portion of the food intake). Mice were euthanized by cervical dislocation after an overnight (16h) fast and tissues for molecular analysis were flash-frozen in liquid nitrogen and stored at -80°C.

Metabolite Extraction

Approximately 30 mg of flash-frozen liver tissue was pulverized in 1 mL of -80°C 80:20 MeOH:H_2O extraction solvent using a motorized tissue grinder and stored on dry ice for 5 minutes. Samples were then centrifuged at 21,100xg at 4°C for 5 minutes. Supernatants were transferred to individual 15 mL conicals after which 0.8 ml of

-20°C 40:40:20 ACN:MeOH:H_2O extraction solvent was used to resuspend the pelleted samples using a motorized tissue grinder. Resuspended samples were stored on wet ice for 5 minutes. Samples were then centrifuged at max speed for 5 minutes at 4°C and supernatants were combined with those collected after the initial extraction. The 40:40:20 ACN:MeOH:H_2O extraction was then repeated as previously described. Combined metabolite extracts were centrifuged at max speed for 5 minutes at 4°C to pellet any potential insoluble debris after which supernatants were transferred to few individual 15 mL conicals. Finally, extracts were dried using a Thermo Fisher Savant ISS110 SpeedVac and resuspended in 150 µL H_2O per 5 mg of the original liver input. Resuspended extracts were centrifuged at max speed for 5 minutes at 4°C after which supernatants were transferred to glass vials for LC-MS analysis.

LC-MS Metabolomics

Prepared metabolite samples were injected in random order onto a Thermo Fisher Scientific Vanquish UHPLC with a a Waters Acquity UPLC BEH C18 column (1.7 µm, 2.1x100mm; Waters Corp., Milford, MA, USA) and analyzed using a Thermo Fisher Q Exactive Orbitrap mass spectrometer in negative ionization mode. LC separation was performed over a 25 minute method with a 14.5 minute linear gradient of mobile phase (buffer A, 97% water with 3% methanol, 10mM tributylamine, and acetic acid-adjusted pH of 8.3) and organic phase (buffer B, 100% methanol) (0 minute, 5% B; 2.5 minute, 5% B; 17 minute, 95% B; 19.5 minute, 5% B; 20 minute, 5% B; 25 minute, 5% B, flow rate 0.2mL/min). A quantity of 10 µl of each sample was injected into the system for analysis. The ESI settings were 30/10/1 for sheath/aux/sweep gas flow rates, 2.50kV for spray voltage, 50 for S-lens RF level, 350C for capillary temperature, and 300C for auxiliary gas heater temperature. MS1 scans were operated at resolution = 70,000, scan range = 85-1250m/z, automatic gain control target = 1 x 10^6, and 100 ms maximum IT. Raw data files were converted into mzml for metabolite identification and peak AreaTop quantification using EI-MAVEN (v0.12.1-beta). Peak AreaTop values were imported into MetaboAnalyst for statistical analysis (one factor) using default settings.

Transcriptomic Analysis

RNA was extracted from liver with TRI Reagent (Thermo Fisher, AM9738), then treated with DNase (Invitrogen, 12185010) and purified with RNA purification kit (Ambion, 12183025). The concentration and purity of RNA was determined using a NanoDrop 2000c spectrophotometer (Thermo Fisher Scientific, Waltham, MA) and RNA was diluted to 100-400 ng/µl for sequencing. The RNA was then submitted to the University of Wisconsin-Madison Biotechnology Center Gene Expression Center & DNA Sequencing Facility, and RNA quality was assayed using an Agilent RNA NanoChip. RNA libraries were prepared using the TruSeq Stranded Total RNA Sample Preparation protocol (Illumina, San Diego, CA) with 250ng of mRNA, and cleanup was done using RNA Clean beads (lot #17225200). Reads were aligned to the mouse (*Mus musculus*) with genome-build GRCm38.p5 of accession NCBI:GCA_000001635.7[DL9] and expected counts were generated with ensembl gene IDs (Zerbino et al., 2018).

Analysis of significantly differentially expressed genes (DEGs) was completed in R version 4.3.0. (Team, 2017) using *edgeR* (Robinson et al., 2010) and *limma* (Ritchie et al., 2015). Gene names were converted to

gene symbol and Entrez ID formats using the *mygene* package. Genes with too many missing values were removed, if genes were present in less than one diet/age group they were removed. To reduce the impact of external factors not of biological interest that may affect expression, data was normalized to ensure the expression distributions of each sample are within a similar range. We normalized using the trimmed mean of M-values (TMM), which scales to library size. Heteroscedasticity was accounted for using the voom function, DEGs were identified using an empirical Bayes moderated linear model, and log coefficients and Benjamini-Hochberg (BH) adjusted p-values were generated for each comparison of interest (Benjamini and Hochberg, 1995). DEGs specific to each condition were rank sorted by log2 fold-change and subsequently used in GSEA Preranked analyses with default settings for gene ontology biological process (GO-BP) pathway enrichment (Subramanian et al., 2005).

Histone Extraction and Chemical Derivatization

Approximately 30 mg of liver tissue was resuspended in 800 µl of ice-cold Buffer A (10 mM Tris-HCl pH 7.4, 10 mM NaCl, and 3 mM MgCl2) supplied with protease and histone deacetylase inhibitors (10 µg/ml leupeptin, 10 µg/ml aprotinin, 100 µM phenylmethylsulfonyl fluoride, 10 mM nicotinamide, 1 mM sodium-butyrate, and 4 µM trichostatin A) followed by 20 strokes of loose- and 20 strokes of tight-pestle homogenization in a 1 mL Wheaton dounce homogenizer and strained through a 100 µM filter before being transferred to a new 1.5 mL Eppendorf tube. Samples were then centrifuged at 800xg for 10 minutes at 4°C to pellet nuclei. Supernatants were transferred to fresh 1.5 mL Eppendorf tubes or discarded. The remaining nuclei pellet was resuspended in 500 µL ice-cold PBS pH 7.4 and centrifuged at 800xg for 10 minutes at 4°C. The supernatant was discarded and nuclei were again washed with 500 µL ice-cold PBS pH 7.4. Next, pelleted nuclei were resuspended in 500 µL of 0.4N H_2SO_4 and rotated at 4°C for 4 hours. Samples were centrifuged at 3,400xg for 5 minutes at 4°C to pellet nuclear debris and precipitated non-histone proteins. Supernatants were transferred to new 1.5 mL Eppendorf tubes after which 125 µL of 100% trichloroacetic acid was added and incubated overnight on ice at 4°C. The next day, samples were centrifuged at 3,400xg for 5 minutes at 4°C to pellet precipitated histone proteins. Supernatants were discarded and precipitant was washed with 1 mL ice-cold acetone +0.1% HCl. Samples were centrifuged at 3,400xg for 2 minutes at 4°C and supernatants were again discarded. This process was repeated with a 100% ice-cold acetone wash. Residual acetone was allowed to evaporate at room temperature for 10 minutes after which dried precipitant was resuspended in H_2O. Finally, samples were centrifuged at 21,100xg for 5 minutes at 4°C to pellet any remaining insoluble debris and supernatants containing purified histone were transferred to new 1.5 mL Eppendorf tubes.

To prepare purified histone samples for LC-MS/MS analysis, 5 µg of each sample were diluted with H_2O to a final volume of 9 µl. 1 µL of 1 M triethylammonium bicarbonate was added to each sample to buffer the solution to a final pH of 7-9. Next, 1 µL of 1:100 d6-acetic anhydride:H2O was added to each sample followed by a 2 minute room temperature incubation. The reaction was quenched via addition of 1 µL 80 mM hydroxylamine followed by a 20 minute room temperature incubation. Next, d3-acetylated histones were digested with 0.1 µg trypsin for 4 hours at 37°C. Upon completion of trypsin digestion, 5 µL of 0.02 M NaOH was added to adjust the final pH to ~9-10. Prepared histone peptides were then N-terminally modified with 1 µL 1:50 phenyl

isocyanate:ACN for 1-hour at 37°C. Modified peptides were desalted and eluted-off of EmporeC18 extraction membrane. Eluted samples were dried completely using a Thermo Fisher Scientific Savant ISS110 SpeedVac and resuspended in 40 µL sample diluent (94.9% H2O, 5% ACN, 0.1% TFA). Resuspended samples were centrifuged at max speed for 5 min at 4°C after which supernatants were transferred to glass vials for LC-MS/MS analysis.

LC-MS/MS Histone Proteomics

Derivatized histone peptides were injected onto a Dionex Ultimate3000 nanoflow HPLC with a Waters nanoEase UPLC C18 column (100 m x 150 mm, 3 µm) coupled to a Thermo Fisher Q-Exactive mass spectrometer at 700 nL/ min. Aqueous phase (A) consisted of H2O + 0.1% formic acid while the mobile phase (B) consisted of acetonitrile + 0.1% formic acid (B). Histone peptides were resolved using the following linear gradient: 0 min, 2.0% B; 5 min, 2.0% B; 65 min, 35% B; 67 min, 95% B; 77 min, 95% B; 79 min, 2.0% B; 89 min, 2.0% B. Data was acquired using data-independent acquisition (DIA) mode. The mass spectrometer was operated with a MS1 scan at resolution = 35,000, automatic gain control target = 1 × 106, and scan range = 390-910 m/z, followed by a DIA scan with a loop count of 10. DIA settings were as follows: window size = 10 m/z, resolution = 17,500, automatic gain control target = 1 × 106, DIA maximum fill time = AUTO, and normalized collision energy = 30.

DIA Thermo .raw files were analyzed via the EpiProfile 2.0 the AcD3 module (Yuan et al., 2018). Subsequent data filtering (i.e., removing samples with (1) >2 null values for common peptides or (2) >50% CV) and normalization was performed using our published Histone Analysis Workflow (Thomas et al., 2020).

Statistics

Most statistical analyses were conducted using Prism, version 9 (GraphPad Software Inc., San Diego, CA, USA), R (version 4.1.0), or MatLab (version R2023b). Tests involving multiple factors were or by one-way ANOVA with Diet as the categorical variable followed by a Tukey–Kramer or Dunnett's *post hoc* test for multiple comparisons as appropriate. Data distribution was assumed to be normal but was not formally tested.

Acknowledgements

The Lamming lab is supported in part by the NIA (AG056771, AG062328, AG081482, and AG084156), the NIDDK (DK125859), and startup funds from UW-Madison. The Denu lab is supported in part by the NIH (GM149279 and DK125859). CLG was supported in part by Dalio Philanthropies, a Glenn Foundation Postdoctoral Fellowship, and by Hevolution Foundation award HF-AGE AGE-009. RB is supported by F31AG081115. The authors used the UW-Madison Biotechnology Center Gene Expression Center (RRID:SCR_017757) which is supported in part by the UWCCC (P30CA014520). This work was supported using facilities and resources from the William S. Middleton Memorial Veterans Hospital. The content is solely the responsibility of the authors and does not necessarily represent the official views of the NIH. This work does not represent the views of the Department of Veterans Affairs or the United States Government.

Conflict of interests

SAH is a consultant for Galilei Biosciences. JMD is a co-founder of Galilei Biosciences and a consultant for Evrys Bio. DWL has received funding from, and is a scientific advisory board member of, Aeovian Pharmaceuticals, which seeks to develop novel, selective mTOR inhibitors for the treatment of various diseases.

Figure Legends

Figure 1: Essential amino acid restriction elicits systemic physiologic responses unique from rapamycin treatment. (*A*) Visual representation of study design. (*B*) Weekly body weight measurements. (*C*) Bar graph illustrating weekly food consumption normalized to mouse body weight values. (*D-E*) Bar graphs depicting absolute changes in lean and fat mass measured via whole-body MRI following three weeks of dietary intervention or rapamycin treatment. (*F-G*) Bar graphs depicting the body composition percentages of lean and fat following three weeks of dietary intervention or rapamycin treatment. (*H-I*) Glucose tolerance test curves and calculated area under the curve (AUC) values. Error bars = SEM; N = 12; * = p-value < 0.05 as measured via Student's t-test.

Figure 2: Central metabolites and auxiliary cofactors are differentially regulated in response to individual dietary EAA restriction or rapamycin treatment. (*A*) Heatmap with hierarchical clustering of metabolite abundance values. (*B*) PCA analysis of log transformed, relative metabolite abundance values. (*C-F*) Diagram depicting log2 fold-changes in metabolite abundance relative to controls within the larger context of their associated metabolic pathways. N = 12 for control, rapamycin, Met-R, and Ile-R groups; N = 11 for Leu-R; p-values measured using default MetaboAnalyst settings.

Figure 3: *Dietary EAA restrictions stimulate unique Histone PTM patterns across all conditions, independent of mTORC1 regulation*. (*A*) Heatmap with hierarchical clustering of stoichiometric histone peptide abundance relative to control values. (*B*) PCA analysis of log transformed, relative histone peptide stoichiometry values. (*C-G*) Bar graphs depicting log2 FC of residue-specific histone PTMs relative to controls. Error bars = standard deviation; N = 12 for control, N = 10 for Rapa; N = 7 for Leu-D; N = 6 for Met-R and Ile-R; * = p-value < 0.05 as measured via Student's t-test.

Figure 4: *Treatment-dependent alterations to liver transcriptional profiles mirror grouping patterns observed in metabolomics analyses with Ile-R stimulating the most significant response*. (*A*) PCA analysis of log transformed gene CPM values. (*B*) Venn diagram of differentially expressed genes with p<0.05. (*C-F*) Volcano plots depicting log2 FC and -log10 adj. p-values for all identified genes. Horizontal marker indicates threshold for statistical significance (p-adj. < 0.05) with significantly changing genes marked in red. (G-J) Dot plots illustrating enriched Gene Ontology – Biological Process (GO-BP) gene sets as determined via Gene

Set Enrichment Analyses (GSEA) of differentially expressed genes unique to each given condition. Example GSEA plots highlighting significantly enriched GO-BP gene groups with positive and negative normalized enrichment scores (NES) are present beneath each corresponding dot plot. N = 12.

References

Arriola Apelo, S.I., Neuman, J.C., Baar, E.L., Syed, F.A., Cummings, N.E., Brar, H.K., Pumper, C.P., Kimple, M.E., Lamming, D.W., 2016. Alternative rapamycin treatment regimens mitigate the impact of rapamycin on glucose homeostasis and the immune system. Aging Cell 15, 28–38. https://doi.org/10.1111/acel.12405

Bellantuono, I., de Cabo, R., Ehninger, D., Di Germanio, C., Lawrie, A., Miller, J., Mitchell, S.J., Navas-Enamorado, I., Potter, P.K., Tchkonia, T., Trejo, J.L., Lamming, D.W., 2020. A toolbox for the longitudinal assessment of healthspan in aging mice. Nat. Protoc. 15, 540–574. https://doi.org/10.1038/s41596-019-0256-1

Benjamini, Y., Hochberg, Y., 1995. Controlling the False Discovery Rate: A Practical and Powerful Approach to Multiple Testing. J. R. Stat. Soc. Ser. B Methodol. 57, 289–300. https://doi.org/10.1111/j.2517-6161.1995.tb02031.x

Buj, R., Chen, C.-W., Dahl, E.S., Leon, K.E., Kuskovsky, R., Maglakelidze, N., Navaratnarajah, M., Zhang, G., Doan, M.T., Jiang, H., Zaleski, M., Kutzler, L., Lacko, H., Lu, Y., Mills, G.B., Gowda, R., Robertson, G.P., Warrick, J.I., Herlyn, M., Imamura, Y., Kimball, S.R., DeGraff, D.J., Snyder, N.W., Aird, K.M., 2019. Suppression of p16 Induces mTORC1-Mediated Nucleotide Metabolic Reprogramming. Cell Rep. 28, 1971-1980.e8. https://doi.org/10.1016/j.celrep.2019.07.084

Cummings, N.E., Williams, E.M., Kasza, I., Konon, E.N., Schaid, M.D., Schmidt, B.A., Poudel, C., Sherman, D.S., Yu, D., Arriola Apelo, S.I., Cottrell, S.E., Geiger, G., Barnes, M.E., Wisinski, J.A., Fenske, R.J., Matkowskyj, K.A., Kimple, M.E., Alexander, C.M., Merrins, M.J., Lamming, D.W., 2018. Restoration of metabolic health by decreased consumption of branched-chain amino acids. J. Physiol. 596, 623–645. https://doi.org/10.1113/JP275075

Fan, J., Krautkramer, K.A., Feldman, J.L., Denu, J.M., 2015. Metabolic regulation of histone post-translational modifications. ACS Chem. Biol. 10, 95–108. https://doi.org/10.1021/cb500846u

Fontana, L., Cummings, N.E., Arriola Apelo, S.I., Neuman, J.C., Kasza, I., Schmidt, B.A., Cava, E., Spelta, F., Tosti, V., Syed, F.A., Baar, E.L., Veronese, N., Cottrell, S.E., Fenske, R.J., Bertozzi, B., Brar, H.K., Pietka, T., Bullock, A.D., Figenshau, R.S., Andriole, G.L., Merrins, M.J., Alexander, C.M., Kimple, M.E., Lamming, D.W., 2016. Decreased Consumption of Branched-Chain Amino Acids Improves Metabolic Health. Cell Rep. 16, 520–530. https://doi.org/10.1016/j.celrep.2016.05.092

Green, C.L., Lamming, D.W., Fontana, L., 2022. Molecular mechanisms of dietary restriction promoting health and longevity. Nat. Rev. Mol. Cell Biol. 23, 56–73. https://doi.org/10.1038/s41580-021-00411-4

Haws, S.A., Yu, D., Ye, C., Wille, C.K., Nguyen, L.C., Krautkramer, K.A., Tomasiewicz, J.L., Yang, S.E., Miller, B.R., Liu, W.H., Igarashi, K., Sridharan, R., Tu, B.P., Cryns, V.L., Lamming, D.W., Denu, J.M., 2020. Methyl-Metabolite Depletion Elicits Adaptive Responses to Support Heterochromatin Stability and Epigenetic Persistence. Mol. Cell 78, 210-223.e8. https://doi.org/10.1016/j.molcel.2020.03.004

Haws, Spencer A., Lillian J. Miller, Diego Rojas La Luz, Vyacheslav I. Kuznetsov, Raymond C. Trievel, Gheorghe Craciun, and John M. Denu. 2023. “Intrinsic Catalytic Properties of Histone H3 Lysine-9

Methyltransferases Preserve Monomethylation Levels under Low S-Adenosylmethionine." *The Journal of Biological Chemistry* 299 (7): 104938. https://doi.org/10.1016/j.jbc.2023.104938.

Hostetler, K. Y., and B. R. Landau. 1967. "Estimation of the Pentose Cycle Contribution to Glucose Metabolism in Tissue in Vivo." *Biochemistry* 6 (10): 2961–64. https://doi.org/10.1021/bi00862a001.

Lee, Min Hee, Craig R. Malloy, Ian R. Corbin, Junjie Li, and Eunsook S. Jin. 2019. "Assessing the Pentose Phosphate Pathway Using [2, 3-13 C2]Glucose." *NMR in Biomedicine* 32 (6): e4096. https://doi.org/10.1002/nbm.4096.

Li, X., Egervari, G., Wang, Y., Berger, S.L., Lu, Z., 2018. Regulation of chromatin and gene expression by metabolic enzymes and metabolites. Nat. Rev. Mol. Cell Biol. 19, 563–578. https://doi.org/10.1038/s41580-018-0029-7

MacArthur, M.R., Mitchell, S.J., Treviño-Villarreal, J.H., Grondin, Y., Reynolds, J.S., Kip, P., Jung, J., Trocha, K.M., Ozaki, C.K., Mitchell, J.R., 2021. Total protein, not amino acid composition, differs in plant-based versus omnivorous dietary patterns and determines metabolic health effects in mice. Cell Metab. 33, 1808-1819.e2. https://doi.org/10.1016/j.cmet.2021.06.011

McCarty, M.F., Barroso-Aranda, J., Contreras, F., 2009. The low-methionine content of vegan diets may make methionine restriction feasible as a life extension strategy. Med. Hypotheses 72, 125–128. https://doi.org/10.1016/j.mehy.2008.07.044

Miller, R.A., Buehner, G., Chang, Y., Harper, J.M., Sigler, R., Smith-Wheelock, M., 2005. Methionine-deficient diet extends mouse lifespan, slows immune and lens aging, alters glucose, T4, IGF-I and insulin levels, and increases hepatocyte MIF levels and stress resistance. Aging Cell 4, 119–125. https://doi.org/10.1111/j.1474-9726.2005.00152.x

Newgard, C.B., An, J., Bain, J.R., Muehlbauer, M.J., Stevens, R.D., Lien, L.F., Haqq, A.M., Shah, S.H., Arlotto, M., Slentz, C.A., Rochon, J., Gallup, D., Ilkayeva, O., Wenner, B.R., Yancy, W.S., Eisenson, H., Musante, G., Surwit, R.S., Millington, D.S., Butler, M.D., Svetkey, L.P., 2009. A branched-chain amino acid-related metabolic signature that differentiates obese and lean humans and contributes to insulin resistance. Cell Metab. 9, 311–326. https://doi.org/10.1016/j.cmet.2009.02.002

Orentreich, N., Matias, J.R., DeFelice, A., Zimmerman, J.A., 1993. Low methionine ingestion by rats extends life span. J. Nutr. 123, 269–274. https://doi.org/10.1093/jn/123.2.269

Richardson, N.E., Konon, E.N., Schuster, H.S., Mitchell, A.T., Boyle, C., Rodgers, A.C., Finke, M., Haider, L.R., Yu, D., Flores, V., Pak, H.H., Ahmad, S., Ahmed, S., Radcliff, A., Wu, J., Williams, E.M., Abdi, L., Sherman, D.S., Hacker, T., Lamming, D.W., 2021. Lifelong restriction of dietary branched-chain amino acids has sex-specific benefits for frailty and lifespan in mice. Nat. Aging 1, 73–86. https://doi.org/10.1038/s43587-020-00006-2

Ritchie, M.E., Phipson, B., Wu, D., Hu, Y., Law, C.W., Shi, W., Smyth, G.K., 2015. limma powers differential expression analyses for RNA-sequencing and microarray studies. Nucleic Acids Res. 43, e47. https://doi.org/10.1093/nar/gkv007

Robinson, M.D., McCarthy, D.J., Smyth, G.K., 2010. edgeR: a Bioconductor package for differential expression analysis of digital gene expression data. Bioinforma. Oxf. Engl. 26, 139–140.

https://doi.org/10.1093/bioinformatics/btp616

Schmidt, J.A., Rinaldi, S., Scalbert, A., Ferrari, P., Achaintre, D., Gunter, M.J., Appleby, P.N., Key, T.J., Travis, R.C., 2016. Plasma concentrations and intakes of amino acids in male meat-eaters, fish-eaters, vegetarians and vegans: a cross-sectional analysis in the EPIC-Oxford cohort. Eur. J. Clin. Nutr. 70, 306–312. https://doi.org/10.1038/ejcn.2015.144

Simcox, J., Lamming, D.W., 2022. The central moTOR of metabolism. Dev. Cell 57, 691–706. https://doi.org/10.1016/j.devcel.2022.02.024

Solon-Biet, S.M., Cogger, V.C., Pulpitel, T., Wahl, D., Clark, X., Bagley, E., Gregoriou, G.C., Senior, A.M., Wang, Q.-P., Brandon, A.E., Perks, R., O'Sullivan, J., Koay, Y.C., Bell-Anderson, K., Kebede, M., Yau, B., Atkinson, C., Svineng, G., Dodgson, T., Wali, J.A., Piper, M.D.W., Juricic, P., Partridge, L., Rose, A.J., Raubenheimer, D., Cooney, G.J., Le Couteur, D.G., Simpson, S.J., 2019. Branched chain amino acids impact health and lifespan indirectly via amino acid balance and appetite control. Nat. Metab. 1, 532–545. https://doi.org/10.1038/s42255-019-0059-2

Son, S.M., Park, S.J., Lee, H., Siddiqi, F., Lee, J.E., Menzies, F.M., Rubinsztein, D.C., 2019. Leucine Signals to mTORC1 via Its Metabolite Acetyl-Coenzyme A. Cell Metab. 29, 192-201.e7. https://doi.org/10.1016/j.cmet.2018.08.013

Subramanian, A., Tamayo, P., Mootha, V.K., Mukherjee, S., Ebert, B.L., Gillette, M.A., Paulovich, A., Pomeroy, S.L., Golub, T.R., Lander, E.S., Mesirov, J.P., 2005. Gene set enrichment analysis: a knowledge-based approach for interpreting genome-wide expression profiles. Proc. Natl. Acad. Sci. U. S. A. 102, 15545–15550. https://doi.org/10.1073/pnas.0506580102

Sun, L., Sadighi Akha, A.A., Miller, R.A., Harper, J.M., 2009. Life-span extension in mice by preweaning food restriction and by methionine restriction in middle age. J. Gerontol. A. Biol. Sci. Med. Sci. 64, 711–722. https://doi.org/10.1093/gerona/glp051

Thomas, S.P., Haws, S.A., Borth, L.E., Denu, J.M., 2020. A practical guide for analysis of histone post-translational modifications by mass spectrometry: Best practices and pitfalls. Methods San Diego Calif 184, 53–60. https://doi.org/10.1016/j.ymeth.2019.12.001

Vermeulen, L., De Sousa E Melo, F., van der Heijden, M., Cameron, K., de Jong, J.H., Borovski, T., Tuynman, J.B., Todaro, M., Merz, C., Rodermond, H., Sprick, M.R., Kemper, K., Richel, D.J., Stassi, G., Medema, J.P., 2010. Wnt activity defines colon cancer stem cells and is regulated by the microenvironment. Nat. Cell Biol. 12, 468–476. https://doi.org/10.1038/ncb2048

Wanders, D., Forney, L.A., Stone, K.P., Burk, D.H., Pierse, A., Gettys, T.W., 2017. FGF21 Mediates the Thermogenic and Insulin-Sensitizing Effects of Dietary Methionine Restriction but Not Its Effects on Hepatic Lipid Metabolism. Diabetes 66, 858–867. https://doi.org/10.2337/db16-1212

White, P.J., Lapworth, A.L., An, J., Wang, L., McGarrah, R.W., Stevens, R.D., Ilkayeva, O., George, T., Muehlbauer, M.J., Bain, J.R., Trimmer, J.K., Brosnan, M.J., Rolph, T.P., Newgard, C.B., 2016. Branched-chain amino acid restriction in Zucker-fatty rats improves muscle insulin sensitivity by enhancing efficiency of fatty acid oxidation and acyl-glycine export. Mol. Metab. 5, 538–551. https://doi.org/10.1016/j.molmet.2016.04.006

Yang, Z., He, M., Austin, J., Sayed, D., Abdellatif, M., 2023. Reducing branched-chain amino acids improves cardiac stress response in mice by decreasing histone H3K23 propionylation. J. Clin. Invest. 133, e169399. https://doi.org/10.1172/JCI169399

Yu, D., Richardson, N.E., Green, C.L., Spicer, A.B., Murphy, M.E., Flores, V., Jang, C., Kasza, I., Nikodemova, M., Wakai, M.H., Tomasiewicz, J.L., Yang, S.E., Miller, B.R., Pak, H.H., Brinkman, J.A., Rojas, J.M., Quinn, W.J., Cheng, E.P., Konon, E.N., Haider, L.R., Finke, M., Sonsalla, M., Alexander, C.M., Rabinowitz, J.D., Baur, J.A., Malecki, K.C., Lamming, D.W., 2021. The adverse metabolic effects of branched-chain amino acids are mediated by isoleucine and valine. Cell Metab. 33, 905-922.e6. https://doi.org/10.1016/j.cmet.2021.03.025

Yu, D., Yang, S.E., Miller, B.R., Wisinski, J.A., Sherman, D.S., Brinkman, J.A., Tomasiewicz, J.L., Cummings, N.E., Kimple, M.E., Cryns, V.L., Lamming, D.W., 2018. Short-term methionine deprivation improves metabolic health via sexually dimorphic, mTORC1-independent mechanisms. FASEB J. Off. Publ. Fed. Am. Soc. Exp. Biol. 32, 3471–3482. https://doi.org/10.1096/fj.201701211R

Yuan, Z.-F., Sidoli, S., Marchione, D.M., Simithy, J., Janssen, K.A., Szurgot, M.R., Garcia, B.A., 2018. EpiProfile 2.0: A Computational Platform for Processing Epi-Proteomics Mass Spectrometry Data. J. Proteome Res. 17, 2533–2541. https://doi.org/10.1021/acs.jproteome.8b00133

Zerbino, D.R., Achuthan, P., Akanni, W., Amode, M.R., Barrell, D., Bhai, J., Billis, K., Cummins, C., Gall, A., Girón, C.G., Gil, L., Gordon, L., Haggerty, L., Haskell, E., Hourlier, T., Izuogu, O.G., Janacek, S.H., Juettemann, T., To, J.K., Laird, M.R., Lavidas, I., Liu, Z., Loveland, J.E., Maurel, T., McLaren, W., Moore, B., Mudge, J., Murphy, D.N., Newman, V., Nuhn, M., Ogeh, D., Ong, C.K., Parker, A., Patricio, M., Riat, H.S., Schuilenburg, H., Sheppard, D., Sparrow, H., Taylor, K., Thormann, A., Vullo, A., Walts, B., Zadissa, A., Frankish, A., Hunt, S.E., Kostadima, M., Langridge, N., Martin, F.J., Muffato, M., Perry, E., Ruffier, M., Staines, D.M., Trevanion, S.J., Aken, B.L., Cunningham, F., Yates, A., Flicek, P., 2018. Ensembl 2018. Nucleic Acids Res. 46, D754–D761. https://doi.org/10.1093/nar/gkx1098

Figure 1 - Essential amino acid restriction elicits systemic physiologic responses unique from rapamycin treatment.

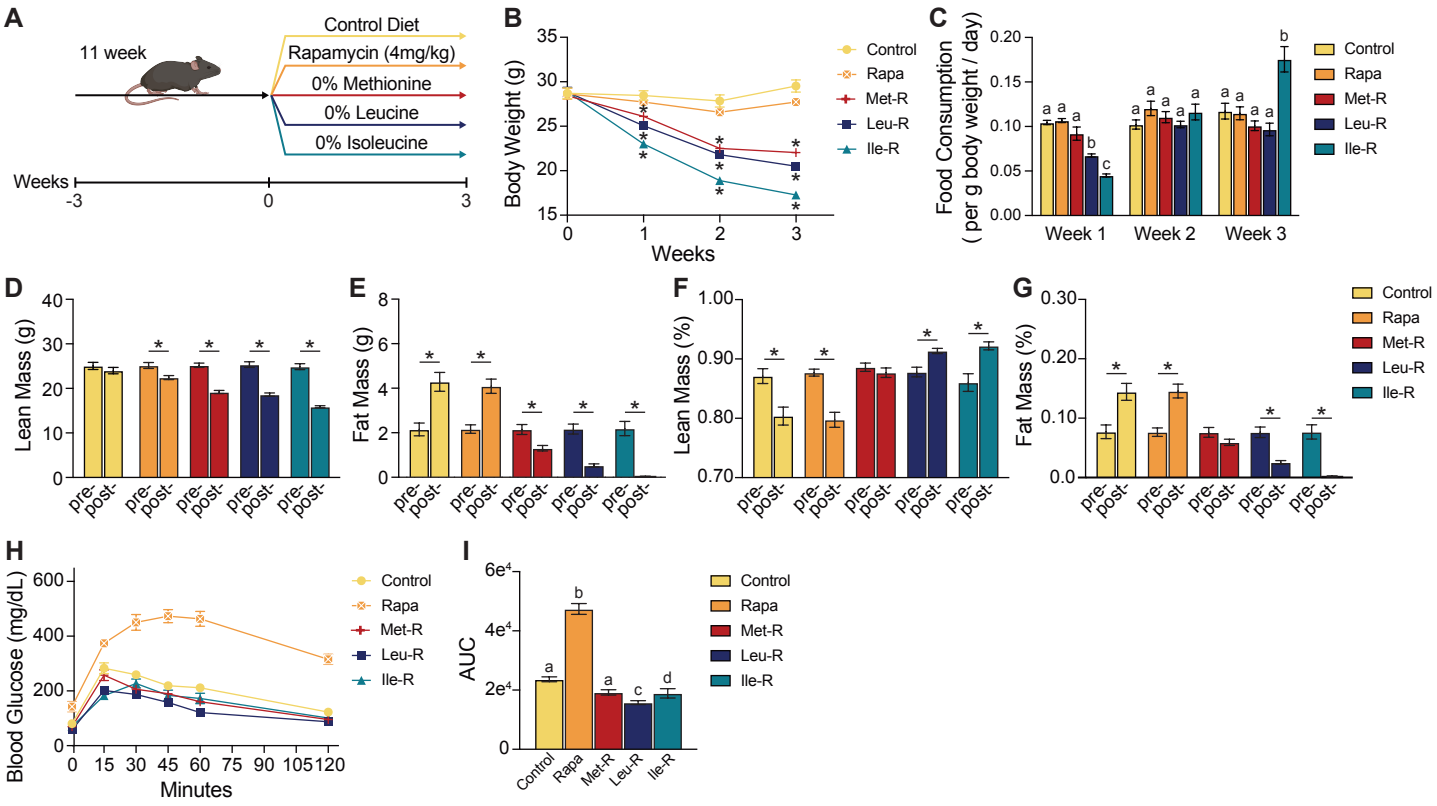

Figure 2 - Central metabolites and auxiliary cofactors are differentially regulated in response to individual dietary EAA restriction or rapamycin treatment.

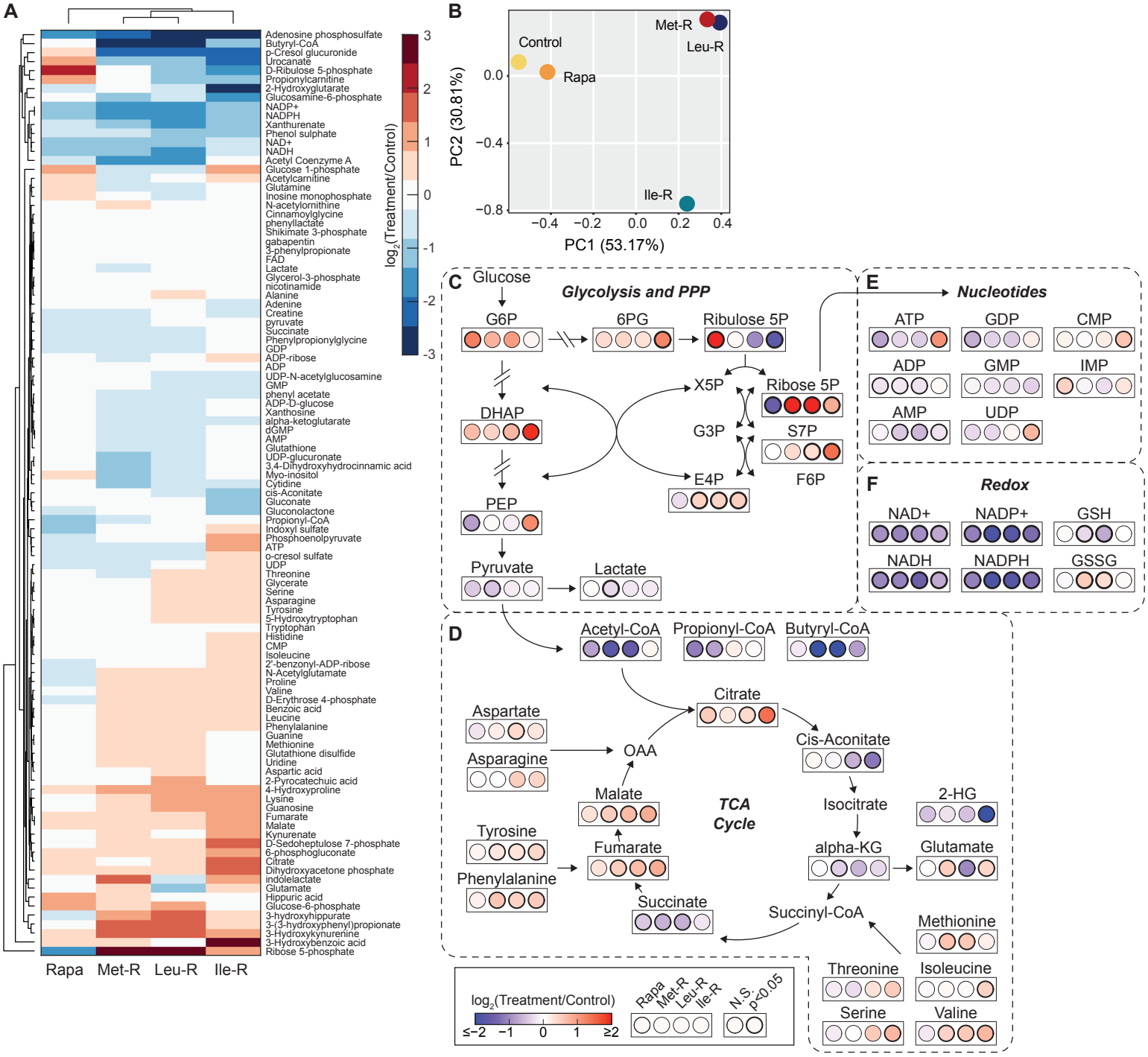

Figure 3 - Dietary EAA restrictions stimulate unique Histone PTM patterns across all conditions, independent of mTORC1 regulation

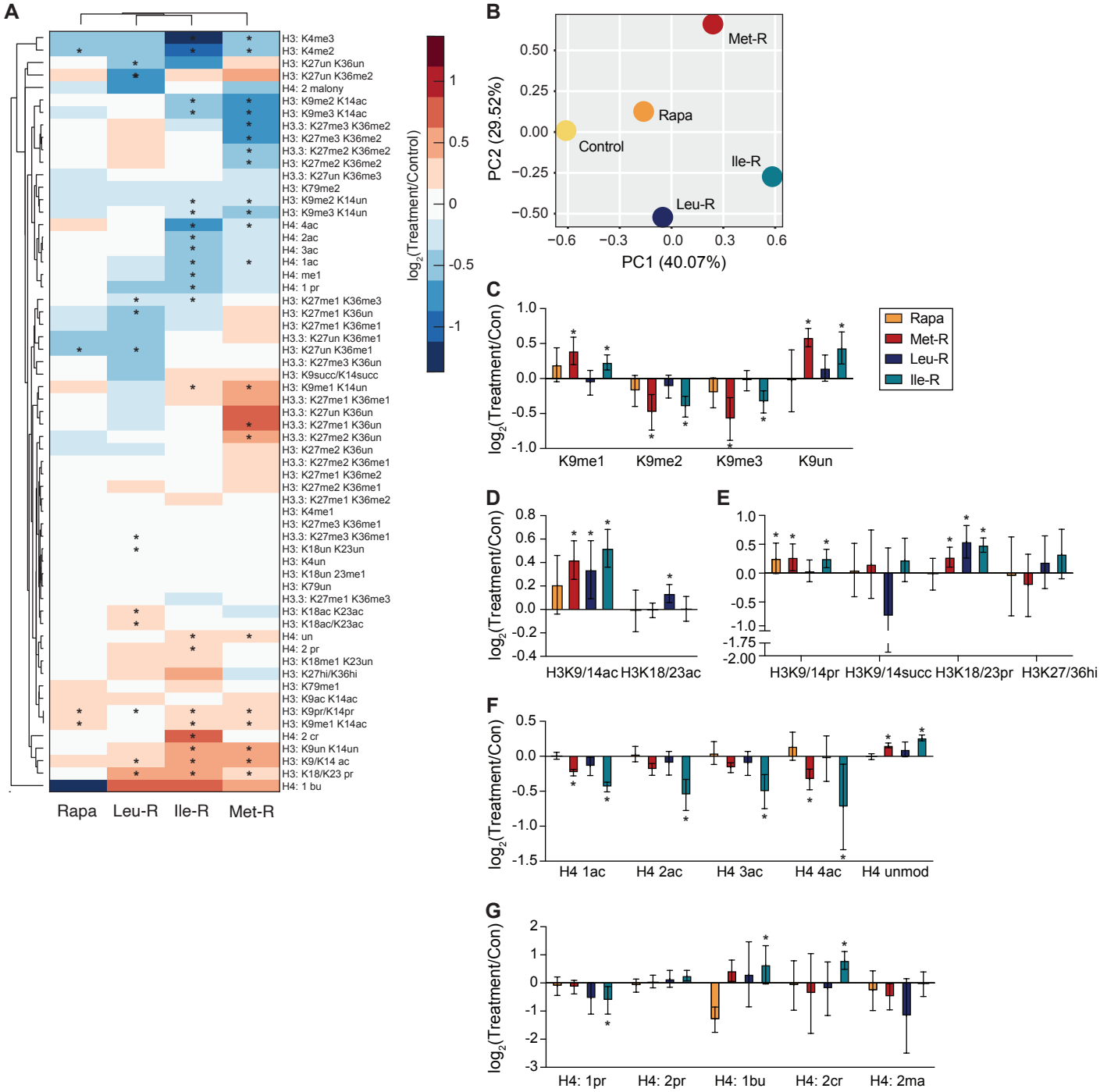
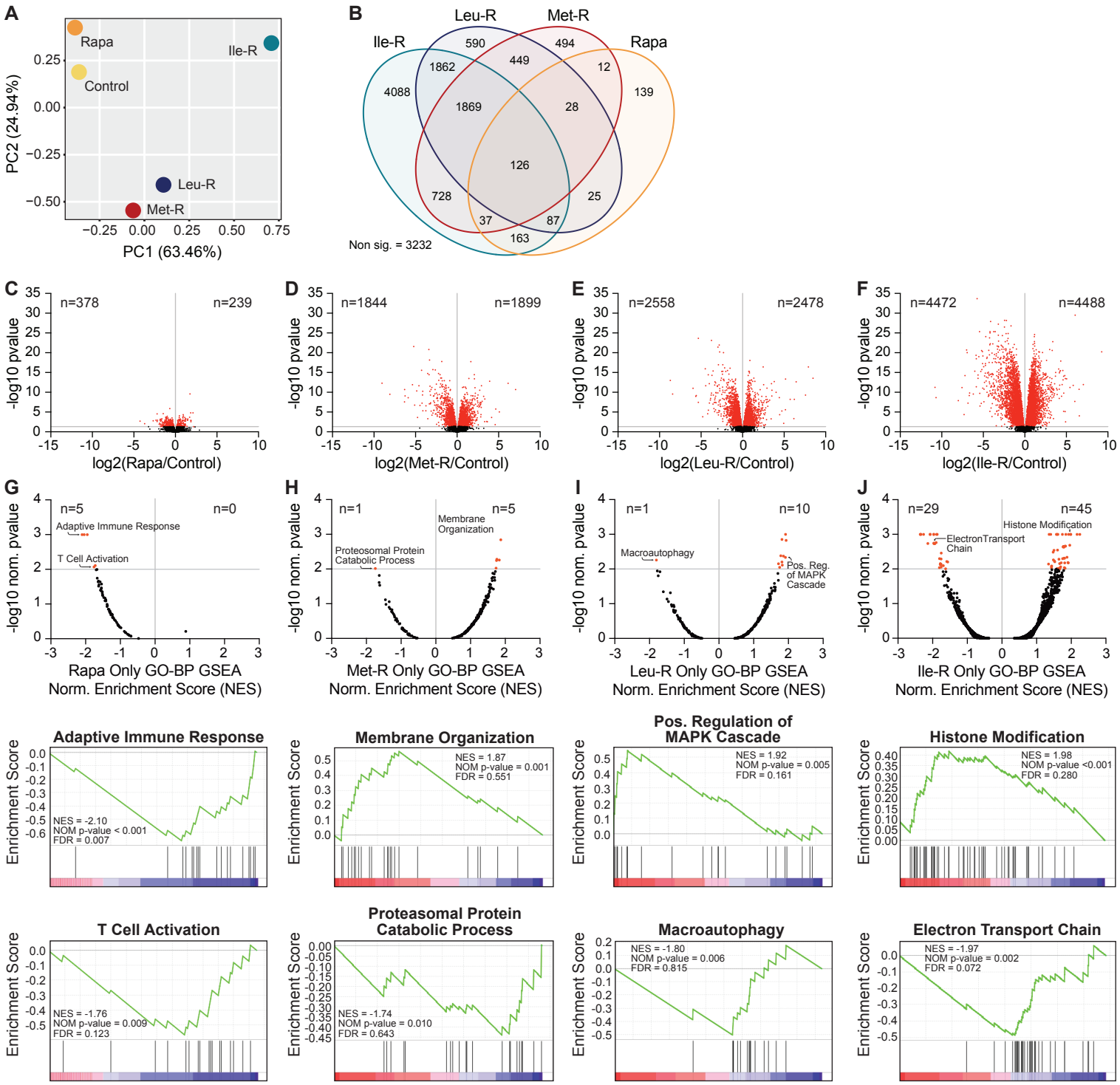
Figure 4 - Treatment-dependent alterations to liver transcriptional profiles mirror grouping patterns observed in metabolomics analyses with Ile-R stimulating the most significant response